Journal of Power Sources 182 (2008) 230–239

Contents lists available at ScienceDirect

Journal of Power Sources

journal homepage: www.elsevier.com/locate/jpowsour

Thermal and mechanical properties of $LaCoO_3$ and $La_{0.8}Ca_{0.2}CoO_3$ perovskites

Nina Orlovskaya[a,*], Mykola Lugovy[a], Siddhartha Pathak[b], David Steinmetz[b], John Lloyd[b], Laura Fegely[b], Miladin Radovic[c], E. Andrew Payzant[d], Edgar Lara-Curzio[d], Larry F. Allard[d], Jakob Kuebler[e]

[a] Department of Mechanical, Materials, and Aerospace Engineering, University of Central Florida, Orlando, FL 32816, USA
[b] Department of Materials Science and Engineering, Drexel University, Philadelphia, PA, USA
[c] Department of Mechanical Engineering, Texas A&M University, College Station, TX 77843, USA
[d] Materials Science and Technology Division, Oak Ridge National Laboratory, Oak Ridge, TN, USA
[e] EMPA, Materials Science and Technology, Laboratory for High Performance Ceramics, Duebendorf, Switzerland

ARTICLE INFO

Article history:
Received 19 February 2008
Accepted 17 March 2008
Available online 3 April 2008

Keywords:
Perovskite
Strength
Fracture toughness
Thermal expansion
Young's modulus

ABSTRACT

In this work, the thermal and mechanical properties such as coefficient of thermal expansion, strength, Young's modulus and fracture toughness of $LaCoO_3$ and $La_{0.8}Ca_{0.2}CoO_3$ perovskites have been studied, as well as slow crack growth of $La_{0.8}Ca_{0.2}CoO_3$. The mechanical performance of the two cobaltites have been evaluated in terms of their ferroelastic hysteresis properties such as non-symmetry in bending of both stress and strain distributions, non-linear deformation upon applied load from the arbitrary low stresses, and ferroelastic toughening.

1. Introduction

The mechanical properties of $LaCoO_3$-based ceramics have received our attention in recent years [1–4] because of their ferroelastic behavior. The thermal performance and mechanical properties such as bending and compressive strength, Young's modulus, fracture toughness, hardness, and coefficient of thermal expansion for both pure and Ca^{2+} and Sr^{2+}-doped cobaltites have been reported earlier [3–5]. In addition, there are several publications on deformation behavior of the cobaltites in compression [1–4,6–8]. It has been demonstrated [1–9] that these materials exhibit a strong ferroelastic behavior, i.e. characteristic nonlinear stress–strain dependence upon loading. Typically, the strength of the $LaCoO_3$ under four-point bending is calculated using the following elastic beam equation:

$$\sigma_c = \frac{3P(s_1 - s_2)}{2bh^2}, \quad (1)$$

where P is the critical load, s_1 is the distance between outer rollers, s_2 is the distance between inner rollers, b is the specimen width, and h is the specimen height. Eq. (1) was used to calculate bending strength although it has been shown [10] that when a ceramic is ferroelastic, the deformation of materials in bending is not symmetric. When asymmetry of the stress distribution on the tensile and compressive surfaces exists, different approaches need to be used for the calculation of stress in the material under non-homogeneous load (for example, a bar in bending [10,11]). If, instead, the classical elastic beam approach is used to calculate failure stress of the cobaltites in bending, i.e. Eq. (1), a significant error can be introduced when designing components with ferroelastic $LaCoO_3$-based ceramics.

This brings us to the question of how to estimate accurately the mechanical properties of ferroelastically deformed ceramics in bending, such as $LaCoO_3$-based perovskites, and determine their stress–strain behavior and Young's modulus. Two different approaches for estimation of the effective Young's modulus of the ferroelastic ceramics can be found in the literature. The Young's modulus is usually reported as the slope of the stress–strain curve at the beginning of the loading, when it is expected that the material will behave in linear elastic manner. For some ferroelectric/ferroelastic ceramics, whose behavior is similar to that of the $LaCoO_3$-based perovskites, the existence of a yield stress σ_0 has been proposed [12] below which the material exhibits a linear stress–strain behavior. Thus, it can be safely assumed that the slope of the stress–strain curve below σ_0 will provide the valid value for Young's modulus. However, another point of view can be found in the literature [13] which states that no σ_0 can be found on the stress–strain curve of a ferroelastic material since the mate-

* Corresponding author. Tel.: +1 4078235770; fax: +1 4078230208.
E-mail address: norlovsk@mail.ucf.edu (N. Orlovskaya).

0378-7753/$ – see front matter © 2008 Elsevier B.V. All rights reserved.
doi:10.1016/j.jpowsour.2008.03.072

rial starts to deform non-linearly from negligibly small stresses. Thus, it is not possible to find any linear portion in the stress–strain curve and this technique cannot provide the true values for the Young's modulus. In that case the secant modulus at appropriate small stresses is usually reported instead of the Young's modulus.

$LaCoO_3$-based ceramics as ferroelastic materials exhibit ferroelastic toughening which is attributed to domain switching at the tip of the propagating crack [14]. The domain switching, among other mechanisms, dissipates energy which causes appearance of the hysteresis on the stress–strain curve. The larger the hysteresis area is, the higher the amount of mechanical energy dissipates leading to the higher the fracture toughness. As a first approximation, the contribution of ferroelasticity to fracture toughness K_{1c} can be presented as [14]:

$$K_{1c} \approx \frac{K_{1c}^0}{\sqrt{1 - 0.16\varepsilon_s E/\sigma_{coer}}}, \quad (2)$$

where K_{1c}^0 denotes toughness in the absence of domain switching, E is the Young's modulus of material, σ_{coer} is the coercive stress and ε_s is the switching strain of polycrystalline material. The decrease of coercive stress causes the increase in the size of the switching zone and consequently the increase in the toughness of ferroelastic material. However, a larger remnant strain corresponds to a larger hysteresis area which in turn means that the larger amount of energy can be dissipated at the crack tip leading to the higher fracture toughness [13]. Finally, the increasing E also results in the fracture toughness enhancement. In this paper, the effect of these three properties on the fracture toughness enhancement of ferroelastic lanthanum cobaltite is further analyzed along with a high temperature dependence of K_{1c}.

Subcritical or slow crack growth (SCG) behavior of lanthanum cobaltites is another phenomenon that has not received enough attention of the scientific community. SCG is a time-dependent process where a crack is growing under a constant load such that the applied stresses are less than that needed for instantaneous fracture [15,16]. The crack grows until it eventually attains a critical load-dependent size at which the strain energy release rate of the specimen exceeds the fracture resistance of the material for unstable fracture to occur and unstable crack extension follows. The importance of SCG behavior lies in the fact that it relates to the cracks naturally present in ceramics which have been introduced during fabrication or processing [16]. Although such studies have been performed on a variety of ceramics [17], to our knowledge there has been no SCG studies done on $LaCoO_3$-based ceramics in the past.

In this work, we report the thermal and mechanical properties of pure $LaCoO_3$ and $La_{0.8}Ca_{0.2}CoO_3$. These two perovskites were studied to determine their thermal expansion, bending stress–strain behavior, elastic modulus, and fracture toughness as a function of temperature. We also report here the SCG behavior of $La_{0.8}Ca_{0.2}CoO_3$ ceramics.

2. Experimental

$LaCoO_3$ and $La_{0.8}Ca_{0.2}CoO_3$ samples were sintered by Praxair Surface Technologies, Specialty Ceramics, USA. After sintering, 2.5 mm × 4 mm × 50 mm bars for bending tests and of ∅6 mm × 12 mm cylinders for compression tests were machined. The polished surface has been thermally etched and the average grain size has been measured by the standard linear intercept technique.

High-temperature X-ray diffraction (HTXRD) data were collected using a PANalytical X'Pert PRO MPD diffractometer with an Anton-Paar XRK-900 high temperature stage. The diffractometer was equipped with an X'celerator detector that allows fast data collection. The data were collected using Cu Kα radiation at 45 kV and 40 mA. Data were collected between 10° and 80° 2θ range with a count time of 30 s so that each scan took less than 5 min. Jade Software (Materials Data Inc., Livermore, CA, USA) was used to identify the XRD peaks from XRD spectrum. The bulk density of all machined specimens was measured by Archimedes method [18]. Fractographic analysis by scanning electron microscopy (SEM) was carried out on selected specimens using Hitachi S-4700 field emission scanning electron microscope.

The thermal mechanical analyzer, TMA, (TMA Q400, TA Instruments, New Castle, DE) was used to measure the thermal expansion of examined cobaltites. Thermal expansion measurements were carried out using 3 mm × 3 mm × 6 mm samples in ambient air in a temperature range of 25–1000 °C. To provide good contact between probe and specimen during the test, a small load of 0.5 N was applied on the specimen via a quartz probe. Usually an average coefficients of thermal expansion (CTE) was determined and used over the temperature range of interest, when thermal expansion changed more or less linearly with temperature. However, to express CTE at each temperature, the so-called instantaneous thermal expansion coefficient, α, as a derivative of the relative length change vs. temperature curve had to be calculated using following relation:

$$\alpha = \frac{1}{L_0}\frac{dL}{dT}, \quad (3)$$

where L is the specimen's length, L_0 is the length at room temperature or initial length of the specimen, and T is a temperature [19]. To calculate the derivative, the recorded dependence of $(L - L_0)$ as a function of T was approximated by a six power polynomial function. Then, the polynomial function was differentiated analytically and the derivative was calculated.

Four-point bending strength was measured using the 4 mm × 3 mm × 45 mm bending bars in the setup with 20 mm loading and 40 mm supporting span. The tests were carried out with a cross-head displacement speed of 1 mm min^{-1} and 0.1 mm min^{-1} at room temperature and 800 °C, respectively, using Universal Testing Machine (UPM-Zwick 1478, Germany) in accordance to EN 843-1 [18]. The room temperature bending tests were carried out using strain gauges mounted to both the tensile and compressive surfaces of the bending bars to monitor directly the compressive and tensile strains on the bending bars. The strain gauges were applied directly in the center of the sample using rapid adhesive. No strain gauges have been used for bending tests at 800 °C.

The Young's modulus was measured using three different methods, namely impulse excitation, four-point bending and compression loading. In the impulse excitation method [20] the Young's modulus was measured at room temperature using a Grindo–Sonic MK 5 (Lemmens, Germany). The Young's modulus at room temperature and 800 °C was also calculated as the secant modulus up to the stress of 9 MPa from strain curves that were obtained in four-point bending tests. As a third comparison, the secant modulus in the range of 0–9 MPa was calculated from stress–strain curve that were determined from uniaxial compression tests at room temperature. Uniaxial compression was performed in a servohydraulic test machine (Instron 8500) with a 20 kN load cell in load control mode with loading rate of 3 MPa s^{-1}.

Dynamic mechanical analysis (DMA) tests were carried out using the Q800 DMA equipment manufactured by TA instruments. Data were recorded both during heating up to 600 °C and cooling down to room temperature at heating/cooling rates of 3 °C min^{-1}. The samples (2.5 mm × 4 mm × 50 mm) were placed in single cantilever fixtures where sample was suspended on two knife-edges and a force was applied from above via a third knife-edge located halfway between the supporting knives. The tests

were carried out in air at frequencies of 10 Hz and amplitude of 2 μm.

Fracture toughness was measured using the single edge V notch beam (SEVNB) method [21]. The notches were inserted using a notching machine and the final notching was made using 1 μm diamond paste and a steel razor blade [21,22]. The cross-head displacement speed of 0.3 mm min^{-1} was used for room temperature measurements (USM, Zwick Z005, Germany) and 0.1 mm min^{-1} for high temperature measurements (Universal Testing Machine UPM-Zwick 1478, Germany). Three specimens of each composition were tested at each temperature.

SCG tests under static loads were performed in ambient air according to the procedure described in [23]. The tests were performed in specifically constructed dead-load apparatus that was insulated from the surrounding vibrations or shocks. The bar-specimens were loaded in four-point flexure with 20 mm loading and 40 mm supporting spans and tested loads that corresponded to the stresses, calculated by elastic beam approach, of 120 MPa, 135 MPa and 150 MPa. Five specimens were tested at each stress level at room temperature. The sample bars were kept under a constant stress at constant temperature 22 °C and humidity (45%) and the time to failure was recorded using an automatic stopwatch built on the machine. For these static lifetime tests a time limit of 168 h (7 days) was chosen as specified in literature [17].

3. Results and discussion

3.1. Thermal expansion

Both $LaCoO_3$ and $La_{0.8}Ca_{0.2}CoO_3$ perovskites were identified to have single-phase rhombohedral ($R\bar{3}c$) structure by X-ray diffraction. No secondary phases were detected in all examined temperature ranges. The lattice parameters determined from high temperature XRD data are presented in Figs. 1 and 2. The *a* and *c* lattice parameters along with unit cell volume as a function of temperature for $LaCoO_3$ are presented in Fig. 1a, c, and e, respectively. While the corresponding CTE values calculated from both the *a* and *c* lattice parameters and the volumetric expansion are presented in Fig. 1b, d, and f, respectively. For comparison, CTE obtained by TMA is also presented (Fig. 1f). Thermal expansion of $LaCoO_3$ heated in air depends on lattice expansion, spin states of Co^{3+} ion, and oxygen vacancies concentration [24]. The spin state transition at about 230 °C causes a large additional Schottky-like contribution to the thermal expansion of $LaCoO_3$ [25]. It was

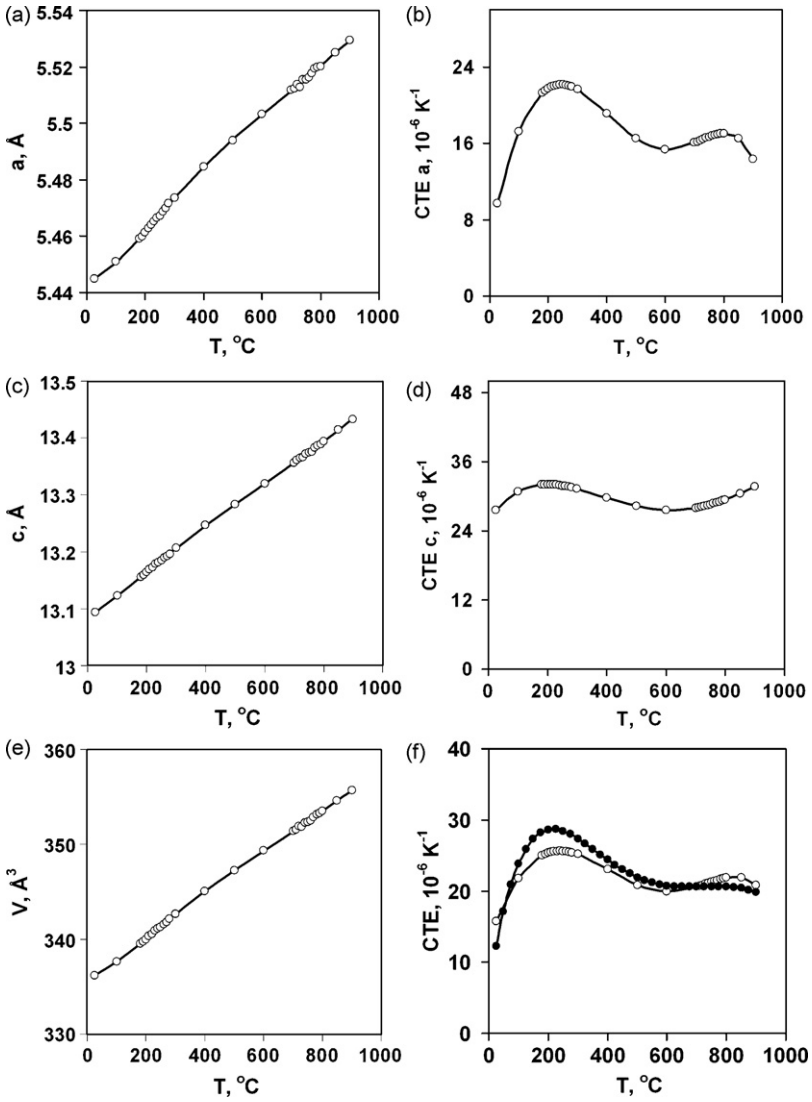

Fig. 1. Results of X-ray powder diffraction for $LaCoO_3$. (a) *a* lattice parameter and (b) CTE in *a* direction as a function of temperature. (c) *c* lattice parameter and (d) CTE in *c* direction as a function of temperature. (e) Elementary cell volume and (f) CTE calculated from cell volume changes (open circles) and TMA measurements (gray circles).

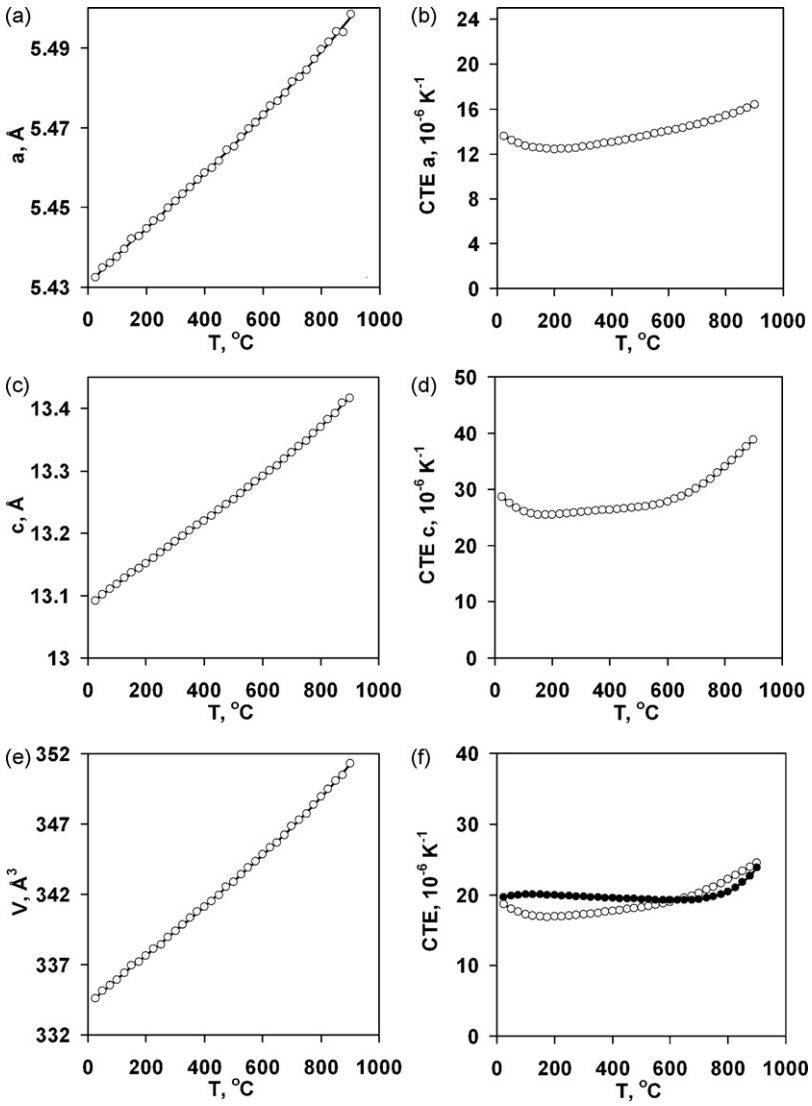

Fig. 2. Results of X-ray powder diffraction for $La_{0.8}Ca_{0.2}CoO_3$. (a) *a* lattice parameter and (b) CTE in *a* direction as a function of temperature. (c) *c* lattice parameter and (d) CTE in *c* direction as a function of temperature. (e) Elementary cell volume and (f) CTE calculated from cell volume changes (open circles) and TMA measurements (gray circles).

reported [26] that intermediate spin (IS) Co^{3+} ion couples strongly with the lattice deformation since it is a Jahn–Teller ion [27]. As well documented by a number of researchers [24,28,29] a sigmoid type CTE plot in the region 150–400 °C can be observed for the lattice expansion in both *a* and *c* directions. The significant increase in CTE from $8 \times 10^{-6}\,K^{-1}$ to $23 \times 10^{-6}\,K^{-1}$ occurs in 25–230 °C temperature range, but at 600 °C the CTE values fall down to $15 \times 10^{-6}\,K^{-1}$ for *a* parameter (Fig. 1b). The CTE values of pure $LaCoO_3$ measured in *c* direction are significantly higher than those measured in *a* direction, but still there is an increase from $28 \times 10^{-6}\,K^{-1}$ to $32 \times 10^{-6}\,K^{-1}$ as temperature increases to 230 °C. Thus, a strong anisotropy of thermal expansion exists as well as nonlinear change in both *a* and *c* directions. The second increase of the CTE is found to occur when the temperature is further increased to 800 °C. CTE calculated using volumetric changes of thermal expansion closely resembles the data obtained using TMA. Comparatively high CTE values of $LaCoO_3$ in 150–400 °C temperature range could be explained by a thermal population of the intermediate spin state of Co^{3+} ions that exists because of the magnetic phase transition in $LaCoO_3$ from low to intermediate spin state at low temperatures [30]. However, the nature of the sigmoid curve is not completely understood since the existence of intermediate spin state Co^{3+} ions cannot explain the significant maximum in CTE at 230 °C. The different explanations for the appearance of the peak CTE value are proposed, such as change in orbital ordering [31], or a second order semiconductor to metal phase transition [32]. However, it is not clear which of these mechanisms is the dominant one for the observed thermal expansion anomaly in the 200–500 °C temperature range.

The Fig. 2 presents the *a* and *c* lattice parameters along with a volume of the unit cell as a function of temperature for $La_{0.8}Ca_{0.2}CoO_3$ composition. Fig. 2 shows that the pronounced maximum in the thermal expansion of the undoped compound, measured by both XRD and TMA methods, is suppressed when $LaCoO_3$ is doped by 20% Ca^{2+}. As doping on A site of a pure $LaCoO_3$ occurs, the significant increase of the CTE in the region of 200–400 °C disappears, and instead a slight decrease of CTE occurs at the beginning of the heating region at ~180 °C in both *a* and *c* directions. The CTE calculated from the volumetric changes closely resemble the CTE curves of *a* and *c* lattice expansions. However, CTE measured by the TMA (gray circles in Fig. 2f) does not show the decrease at ~180 °C. At higher temperatures (from ~700 °C) there

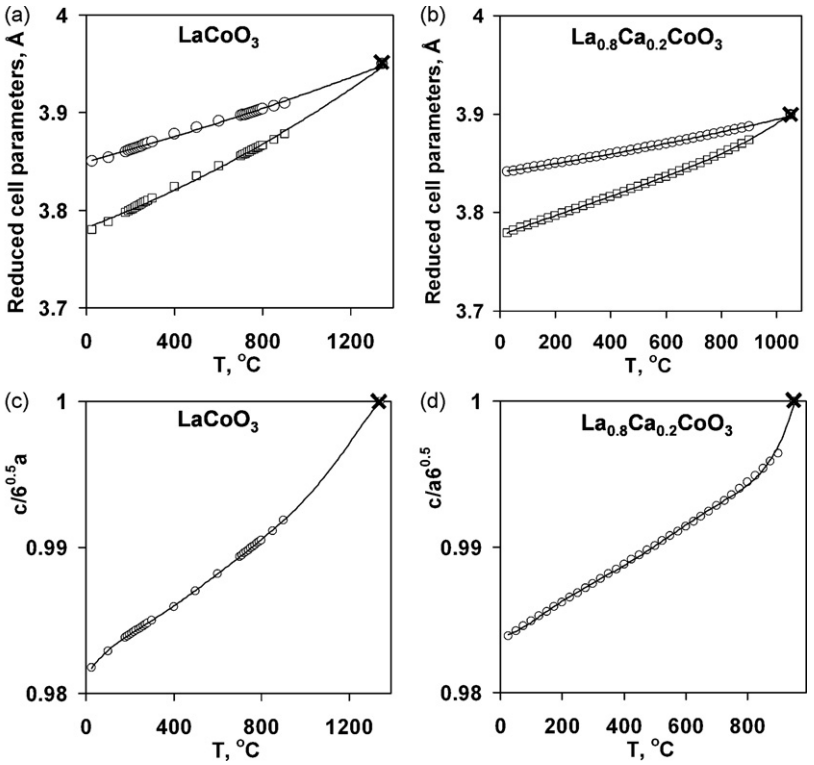

Fig. 3. The temperature variation of the lattice parameters of $LaCoO_3$ (a) and $La_{0.8}Ca_{0.2}CoO_3$ (b) rhombohedral phase. The reduced cell parameters; $a/\sqrt{2}$ (circles) and $c/\sqrt{12}$ (squares) are shown in (a) and (b). (×) The rhombohedral, *r*, to cubic, *c*, transition temperatures of $LaCaO_3$ and $La_{0.8}Ca_{0.2}CoO_3$ reported in Refs. [37,33], respectively. The $c/a\sqrt{6}$ ratio of lattice parameters of the hexagonal phase for (c) $LaCaO_3$ and (d) $La_{0.8}Ca_{0.2}CoO_3$ as a function of temperature demonstrate the level of the rhombohedral distortion.

is a noticeable increase in the CTE values determined in both *a* and *c* directions as well as from the volumetric unit cell changes and the TMA measurements. It is known that doping of $LaCoO_3$ with divalent Ca^{2+} cation generates a large amount of oxygen vacancies in the perovskite lattice. Their amount becomes even higher as temperature is increased [33]. Thus, the formation of the oxygen ion vacancies can be considered to be the major reason for a significant increase of CTE of $La_{0.8}Ca_{0.2}CoO_3$ at temperatures above 800 °C. When oxygen vacancies are formed at high temperature the columbic repulsion between the neighboring B-site cations can be induced which in turn results in an additional expansion of the crystal lattice [34]. In addition, when large quantities of the vacancies are formed, the charge neutrality is maintained by the reduction of Co^{3+} to the lower valence state, which results in the increase of average ionic radius of the Co ions and consequent lattice expansion. The thermal expansion of $La_{0.8}Ca_{0.2}CoO_3$ is very high in the *c* direction and at 900 °C the CTE could reach $40 \times 10^{-6}\,K^{-1}$.

The *c*/*a* ratios of $LaCoO_3$ and $La_{0.8}Ca_{0.2}CoO_3$ as a function of temperature, Fig. 3, were analyzed in the similar way as it was done previously for $LaAlO_3$, $PrAlO_3$, and $NdAlO_3$ in [35]. The $c/a\sqrt{6}$ ratio provides a measure of the rhombohedral distortion and therefore, it is directly related to the spontaneous strains in the cobaltites. As it can be seen in Fig. 3, the rhombohedral distortion is higher for pure $LaCoO_3$ than for that doped with 20% Ca. The $c/a\sqrt{6}$ ratio is reported to be equal to 0.9817 at room temperature for $LaCoO_3$ which is in a rather good agreement with the value of 0.9821 reported earlier in the literature [36]. For $La_{0.8}Ca_{0.2}CoO_3$, $c/a\sqrt{6}$ was found to be 0.9839. Extrapolation of the experimental data to the temperature where $c/a\sqrt{6}$ becomes unity and the material becomes ideal cubic shows that the rhombohedral to cubic ($r \rightarrow c$) transition could occur clearly well above 1000 °C for pure $LaCoO_3$ [37], but 20% Ca doping will lower that transition to around 950 °C [33,38]. This is in good agreement with earlier observations [34] that the greater rhombohedral distortion at room temperature results in the higher transition temperature to cubic structure.

3.2. Strength

In order to derive the pure tensile and compression behavior of the cobaltites in bending, the strain was measured during the loading at room temperature on both surfaces under tension and under compression using strain gages. This allowed the actual stress on the surface to be calculated. The stress–strain curves at room temperatures in Fig. 4a and b were calculated using Nadai approach [10,11]. For comparison the stress–strain curves calculated using the elastic beam approach are also shown in Fig. 4a and b as gray lines. Since it is known that $LaCoO_3$-based perovskites exhibit nonlinear deformation behavior, it is expected that the deformation under bending is non-symmetric, where the absolute value of stresses on surface in tension exceeds that on surface under compression for a given stress level [10]. The absolute value of the strain calculated for the tensile surface of the specimens is indeed larger than the strain calculated for compressive surface for a given stress, and the difference between them increases with stress increase. The critical tensile stress measured from the surface under tension is 86 MPa for $LaCoO_3$ and 98 MPa for $La_{0.8}Ca_{0.2}CoO_3$. Since the compressive strength of cobaltites is rather high and can exceed 1.1 GPa, it is the lower tensile stress which causes the material to fail, and thus, it is the limiting design stress for these materials. Therefore, the critical tensile stress is a true failure stress measured on the surface under tension. The inflection point at 68 MPa could be detected on the compressive surface stress–strain deformation curve of $LaCoO_3$, which coincides with a position of the inflection point measured in uniaxial compression experiments [3]. However, no such inflection point can be found when we use the elastic beam equation for stress calculation for $LaCoO_3$ (Fig. 4a). The inflection point

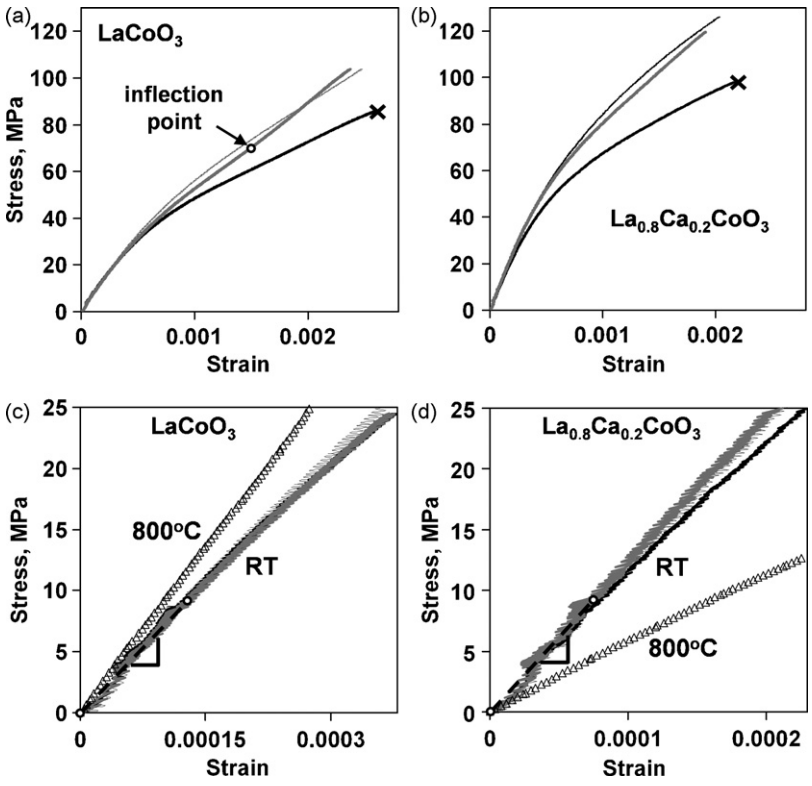

Fig. 4. Stress–strain diagrams of $LaCoO_3$ (a) and $La_{0.8}Ca_{0.2}CoO_3$ (c) in four-point bending at room temperature. (c and d) Magnified initial parts of curves shown in (a) and (b), respectively as well as results obtained at 800 °C (triangles). Thin uppermost curves obtained at room temperature and at 800 °C correspond to stress calculated using elastic beam approach. The results obtained using stain gauges on tensile (black) and compressive (gray) surfaces at room temperature are shown as bold (lowermost) lines for true stress on tensile surface and gray curve for true stress on compressed surface. (×) Corresponds to true failure stress.

for $La_{0.8}Ca_{0.2}CoO_3$ composition is around 140 MPa, as determined in compression experiments elsewhere [3] and thus, it cannot be found in bending since failure of the sample occurred at the lower stress level. The bending strength of $LaCoO_3$ and $La_{0.8}Ca_{0.2}CoO_3$ at 800 °C measured without strain gauges is reported to be equal to 109 ± 19 MPa and 91 ± 4 MPa using the elastic beam equation for strength calculations, respectively.

The fracture surfaces of $LaCoO_3$ and $La_{0.8}Ca_{0.2}CoO_3$ samples tested at room temperature and 800 °C reveal a small amount of porosity. The porosity of the two compositions was in the range of 4–7% and the grain size was measured to be in the range of 2–5 μm. The fracture of $LaCoO_3$ has a mixed, transgranular and intergranular character at both room and high temperatures (Fig. 5a and c). The fracture of $La_{0.8}Ca_{0.2}CoO_3$ perovskite has a pure transgranular character with no separate grains visible on the fracture surfaces at room temperature (Fig. 5b), while at 800 °C the fracture mode was almost intergranular with well-revealed faceted grains and only small areas of the transgranular mode were present (Fig. 5d).

3.3. Young's modulus

The initial slopes of the stress–strain curves, calculated using the elastic approach, are almost the same when measured from the tensile and compressive surfaces in bending. The Young's moduli E were determined as secant moduli from the 0 MPa to 9 MPa (Fig. 4). Though it is not clearly visible in Fig. 4c and d, it is important to notice that the secant modulus has a small deviation from the initial slope of the stress–strain curves even at such small stress as 5–9 MPa. For comparison, the results of the E modulus measurement using natural frequencies method and uniaxial compression are also presented in Fig. 6. E determined by natural frequencies technique shows the highest values of 76 GPa and 141 GPa for $LaCoO_3$ and $La_{0.8}Ca_{0.2}CoO_3$ perovskites respectively, which is expected to be the most accurate modulus value among the three techniques used in this paper [39]. While the E values calculated from bending and uniaxial compression data are lower (which reflect the softening of the materials due to domain wall movement) the differences between the Young's moduli measured by three different techniques are not very high. The surprising result is that the slope of the stress–strain curve of $LaCoO_3$ obtained at 800 °C, Fig. 4c, gives secant modulus of 95 GPa which is higher than the obtained at room temperature, while the secant modulus for $La_{0.8}Ca_{0.2}CoO_3$ perovskite is around 60 GPa at 800 °C and is significantly lower that that at room temperature, as it would be expected. The bulk modulus value of $LaCoO_3$ at room temperature was reported to be 122 GPa [40], thus, using the $E = 76$ GPa measured in the present work, the shear modulus value of 27 GPa and Poisson's ratio value of 0.4 have been calculated for pure $LaCoO_3$.

The decrease of the Young's modulus of $LaCoO_3$ with increase of the temperature due to a lattice softening has been reported earlier in the literature [26] although the reported values of E for $LaCoO_3$ ($E - 100$ GPa at RT) are higher than those determined in the present work ($E - 76$ GPa at RT). The difference in the Young's modulus could be due to difference in the porosity level of the samples, although no data on the porosity of the $LaCoO_3$ was provided in previous study [26]. The lattice softening in the RT—400 °C temperature interval, similar to the one reported in [26] for $LaCoO_3$, is also observed both for pure $LaCoO_3$ (Fig. 7a) and for $La_{0.8}Ca_{0.2}CoO_3$ (Fig. 7b) in the present work. A real part of the dynamic Young's modulus, consisting of the real and imaginary components referred to as the storage and loss moduli, respectively, shows a significant decrease for both perovskites as temperature increases from room

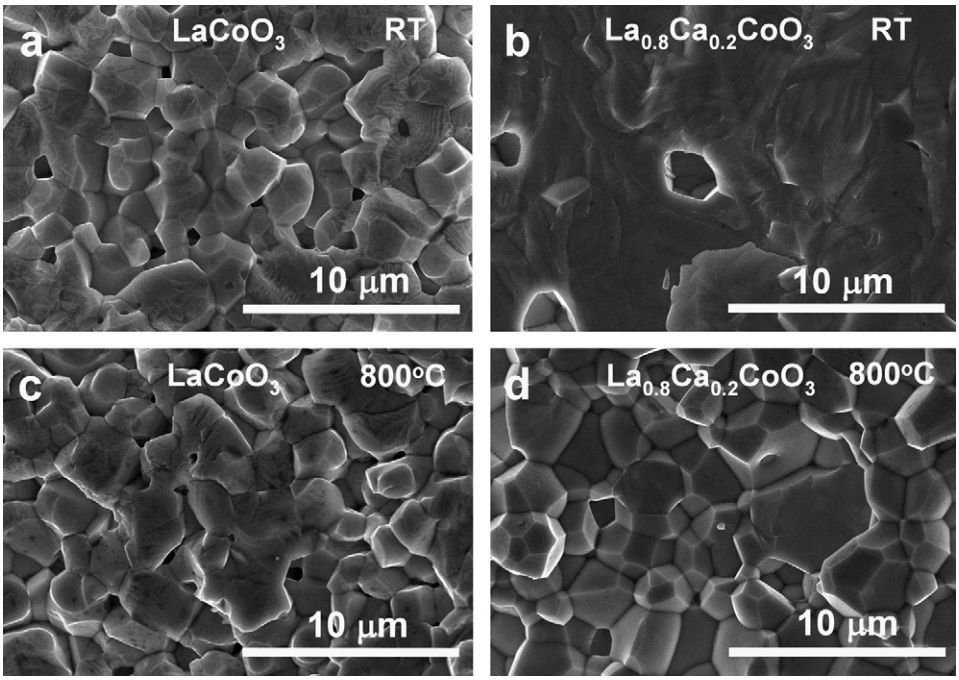

Fig. 5. Fracture surface of $LaCoO_3$ (a) and $La_{0.8}Ca_{0.2}CoO_3$ (b) at room temperature and $LaCoO_3$ (c) and $La_{0.8}Ca_{0.2}CoO_3$ (d) at 800 °C.

temperature to 400 °C. Similar rapid decrease in storage modulus reported for $LaAlO_3$ perovskite [41] has been explained by gradual unfreezing of the domain walls, and it is well known that $LaCoO_3$-based perovskites are also heavily twinned [2]. The anomaly of the storage modulus vs. temperature behavior of pure $LaCoO_3$ can be seen in 90–100 °C temperature region where the small deviation from gradual softening of the lattice is observed (Fig. 7a). Above 400 °C, the storage modulus of $LaCoO_3$ increases rapidly with temperature up to the 600 °C that is the maximum temperature at which DMA experiments could be performed. Thus, it is also possible that a storage modulus at 800 °C of $LaCoO_3$ is higher than that at room temperature, as in the case of secant modulus that was obtained from four-point bending tests.

3.4. Fracture toughness

The reported values of RT fracture toughness of pure $LaCoO_3$ were lower than those measured at RT for $La_{0.8}Ca_{0.2}CoO_3$ [3]. The higher K_{1c} values of $La_{0.8}Ca_{0.2}CoO_3$ at RT have been related to the larger hysteresis loop area observed in this perovskite that those

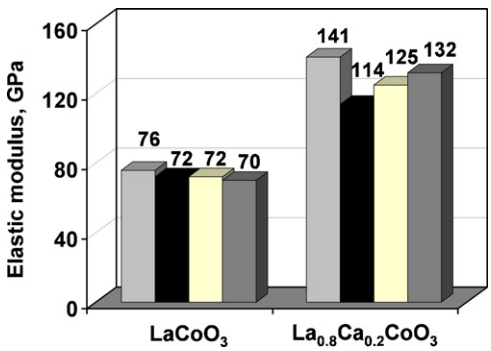

Fig. 6. Elastic modulus of $LaCoO_3$ and $La_{0.8}Ca_{0.2}CoO_3$ determined by different methods: (▢) natural frequencies; (■) bending on tensile surface; (□) bending on compressive surface; (▣) uniaxial compression.

measured for pure $LaCoO_3$. Thus, much larger energy absorption occurs during the deformation of Ca-doped cobaltite leading to the increase of the fracture toughness.

The fracture toughness for both compositions is presented as a function of temperature in Fig. 7c and d. For $LaCoO_3$ the measured fracture toughness decreases from 1.23 MPa $m^{1/2}$ at room temperature to 0.93 MPa $m^{1/2}$ at 260 °C (Fig. 7c). Above 260 °C, the fracture toughness increases again up to 1.05 MPa $m^{1/2}$ at 700 °C, and remains constant above that temperature. For $La_{0.8}Ca_{0.2}CoO_3$ the measured fracture toughness decreases from 1.92 MPa $m^{1/2}$ at room temperature to 0.78 MPa $m^{1/2}$ at 550 °C (Fig. 7d). Above 550 °C, the fracture toughness increases to 1.14 MPa $m^{1/2}$ at 800 °C. Surprisingly or not, but K_{1c} vs. temperature dependence both for $LaCoO_3$ and $La_{0.8}Ca_{0.2}CoO_3$ closely resemble the storage modulus vs. temperature curves. So there is a direct correlation, as one would expect, between lattice softening and brittleness of the cobaltites. The mechanisms responsible for observed increase of K_{1c} with temperature for both $LaCoO_3$ and $La_{0.8}Ca_{0.2}CoO_3$ and elastic modulus for $LaCoO_3$ above 400 °C require further studies. At this point we can only suggest that the higher concentration of oxygen vacancies at higher temperatures influence an increase in K_{1c} values of $La_{0.8}Ca_{0.2}CoO_3$ ceramics regardless observed decrease in elastic modulus and continuous softening.

The effect of the domain switching on increase in fracture toughness of the cobaltites can be roughly estimated using Eq. (2) since all needed materials' parameters are known (Table 1). The switching strain ε_s can be determined from extrapolating strain back to zero stress using the initial unloading slope at maximum stress value of the stress–strain curve measured in compression [3,42]. E values measured by the impulse excitation technique were also available in this paper, as well as a coercive stress as a stress of the inflection point on the loading part of the stress–strain curve measured in compression. In the absence of domain switching, K^0_{1c} was estimated to be 1.16 MPa $m^{1/2}$ for $LaCoO_3$ and 1.79 MPa $m^{1/2}$ for $La_{0.8}Ca_{0.2}CoO_3$ using Eq. (2). This gives 6–7.5% of the relative increase ($\Delta K_{1c} = 100(K_{1c} - K^0_{1c})/K^0_{1c}$) of the fracture toughness due to domain switching toughening mechanism.

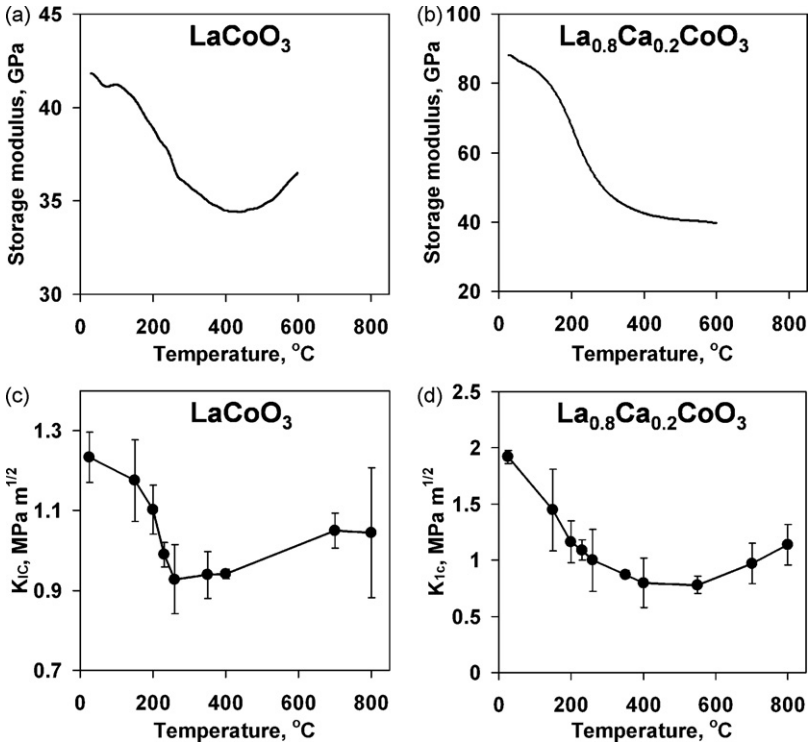

Fig. 7. The storage modulus of $LaCoO_3$ (a) and $La_{0.8}Ca_{0.2}CoO_3$ (b) as a function of temperature measured using DMA. Fracture toughness of $LaCoO_3$ (c) and $La_{0.8}Ca_{0.2}CoO_3$ (d) as a function of temperature.

3.5. Static subcritical (or slow) crack growth

The static subcritical crack growth for $La_{0.8}Ca_{0.2}CoO_3$ was carried out at 22 °C and 55% humidity. The stresses applied are plotted against the resulting lifetimes in a log(time to failure)–log(stress) diagram in Fig. 8. The value for n of this curve, where $-1/n$ is the slope of the straight line joining the median values for time to failure at each static stress level, was found to be 23. A better accuracy for the value of n can potentially be obtained by using a larger sample size at each stress level and also by testing at many more stress levels. However, since static SCG experiments are severely limited by the time needed for each test (at 7 days of testing per sample, Fig. 8 already represents over 2 months worth of testing and data analysis), the present sample-set of five samples at three different stress levels was chosen as the minimum sample size that would generate meaningful SCG data while still maintaining a reasonable time frame for the completion of the tests. Literature values for n for some ceramics such as Al_2O_3 have been reported to be between 50 and 70 [16,43]. In another work, the value of n for $La_{0.8}Sr_{0.2}Ga_{0.8}Mg_{0.2}O_3$ (LSGM) perovskites can be found to be much lower, i.e. around 15 [44]. Thus, the n values for $La_{0.8}Ca_{0.2}CoO_3$, although higher than that of LSGM, is still quite low, suggesting that this material is highly susceptible to SCG when comparing to other ceramics.

For the use of $La_{0.8}Ca_{0.2}CoO_3$ in applications like SOFCs, one of the primary questions of interest is the estimation of the admissible tensile stress for a stipulated minimum lifetime period. When SCG is the dominant failure mechanism, the plot shown in Fig. 8 can be used to answer that question, since it allows us to calculate the maximum stresses at which 50% of samples will fail within the required lifetime period. Another query of interest is estimating of the lifetime of the component when the stresses are known. In that case, the plot shown in Fig. 8 can also provide the time to

Table 1
Calculated fracture toughness in the absence of domain switching and relative increase of fracture toughness due to domain switching

Parameters	$LaCoO_3$	$La_{0.8}Ca_{0.2}CoO_3$
ε_s	0.00646	0.00836
E (GPa)	76	141
σ_{coer} (MPa)	70	140
$\varepsilon_s E/\sigma_{coer}$	7.01	8.42
K_{1c} (MPa m$^{1/2}$)	1.23	1.92
K^0_{1c} (MPa m$^{1/2}$)	1.16	1.79
ΔK_{1c} (%)	6.1	7.5

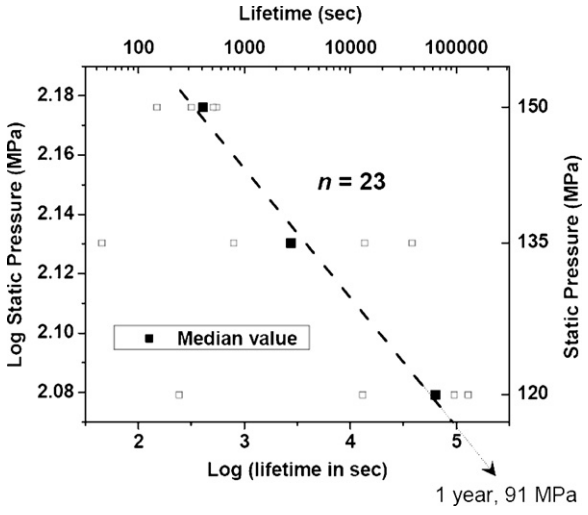

Fig. 8. Log–log diagram of compressive load for static subcritical crack growth vs. lifetime of $La_{0.8}Ca_{0.2}CoO_3$ samples at 22 °C and 55% humidity. Samples were tested at three static stress levels of 120 MPa, 135 MPa and 150 MPa.

failure for 50% of the samples at the given stress level. It should be emphasized here that these lifetime predictions are valid for parts that are approximately of the same size as the specimens tested and examined under similar environmental conditions. Since the effective surface of $La_{0.8}Ca_{0.2}CoO_3$ in an actual SOFC is considerably larger, the tolerable stresses, and the attainable lifetimes, are expected to be even lower in practice. The exact dimensions and the stress distributions need to be known as well if exact calculations are to be made. Tests at higher temperatures (~800 °C) also need to be carried out to ascertain the SCG behavior of the samples at their intended operating temperatures in SOFCs and high temperature oxygen separation membranes.

4. Conclusions

The thermal and mechanical properties, such as thermal expansion, strength, Young's modulus, fracture toughness, and SCG behavior of $LaCoO_3$ and $La_{0.8}Ca_{0.2}CoO_3$ ceramics have been studied. The results of our study are summarized below:

1. The sigmoid type curves are obtained for the instantaneous coefficient of thermal expansion of pure $LaCoO_3$ measured by both XRD and TMA as a function of temperature. Adding of 20% Ca to $LaCoO_3$ completely depresses the anomalous thermal expansion in 200–400 °C region, however, it contributes to the charge disproportionation of Co ions and creates large quantities of oxygen vacancies at high temperatures thus, significantly increasing CTE of $La_{0.8}Ca_{0.2}CoO_3$ above 800 °C.
2. $c/a\sqrt{6}$ ratio of the hexagonal reduced lattice parameters as a function of temperature for $LaCoO_3$ and $La_{0.8}Ca_{0.2}CoO_3$ composition is reported. The $c/a\sqrt{6}$ ratio is larger for pure $LaCoO_3$ at room temperature as compared to $La_{0.8}Ca_{0.2}CoO_3$ but decreases as temperature rises.
3. Non-linear ferroelastic deformation of $LaCoO_3$ and $La_{0.8}Ca_{0.2}CoO_3$ in bending leads to the nonsymmetrical strain distribution upon loading and the absolute value of tensile strain is reported to be larger than that at the compressive surface for a given stress level. The critical tensile stress determined here is a true failure stress measured on the surface under tension.
4. Values of Young's moduli of $LaCoO_3$ and $La_{0.8}Ca_{0.2}CoO_3$ measured by impulse excitation technique as well as a secant modulus in 0–9 MPa stress range determined from stress–strain deformation curves in bending and uniaxial compression show quite good coincidence and correspondence. It is reported that $LaCoO_3$ has E modulus in the range 70–76 GPa and $La_{0.8}Ca_{0.2}CoO_3$ has E modulus in the range of 114–141 GPa at room temperature.
5. The real part of the dynamic Young's modulus, i.e. the storage modulus, shows a remarkable softening in 150–400 °C temperature range for both compositions. Since $K_{1c} \propto E$, the decrease in K_{1c}, is directly proportional to the decrease in storage modulus. A slight increase in K_{1c} at 700–800 °C is observed.
6. Since both materials are ferroelastic, the estimation of toughening due to domain switching toughening mechanism can be made. For the rough estimation, there is only 6% of toughness enhancement due to domain switching for $LaCoO_3$ and 7.5% of toughness enhancement for $La_{0.8}Ca_{0.2}CoO_3$.
7. $La_{0.8}Ca_{0.2}CoO_3$ perovskite is found to be highly susceptible to the SCG. For the stress value of 100 MPa, calculated using elastic approach, the time to failure of 50% of the tested samples would be only ~44 days.

Acknowledgements

This research was supported by NSF, DMR (project #0201770) and in part by an appointment to the Department of Energy's Faculty and Student Team program. This research was also supported in part by the Assistant Secretary for Energy Efficiency and Renewable Energy, Office of FreedomCAR Vehicle Technologies, as a part of the High Temperature Materials Laboratory User Program, Oak Ridge National Laboratory, managed by UT—Battelle, LLC, for the US Department of Energy under contract #DE-AC-05-00OR22725. S. Pathak was supported by 2005 SURA-ORNL (Oak Ridge National Lab) Summer Cooperative Research Program scholarship for this research. We also acknowledge gratefully Roland Bächtold, EMPA, Duebendorf, Switzerland for his help in mechanical testing.

References

[1] K. Kleveland, N. Orlovskaya, T. Grande, A.M.M. Moe, M.-A. Einarsrud, K. Breder, G. Gogotsi, J. Am. Ceram. Soc. 84 (2001) 2029–2033.
[2] N. Orlovskaya, N. Browning, A. Nicholls, Acta Mater. 51 (2003) 5063–5071.
[3] N. Orlovskaya, Y. Gogotsi, M. Reece, B. Cheng, I. Gibson, Acta Mater. 50 (2002) 715–723.
[4] N. Orlovskaya, K. Kleveland, T. Grande, M.-A. Einarsrud, J. Eur. Ceram. Soc. 20 (2000) 51–56.
[5] M. Kriener, M. Braden, D. Senff, O. Zabara, T. Lorenz, J. Magn. Magn. Mater. 310 (2007) e187–e189.
[6] K. Wiik, A. Fossdal, L. Sagdahl, H. Lein, M. Menon, S. Faaland, I. Waernhus, N. Orlovskaya, M.-A. Einarsrud, T. Grande, in: N. Orlovskaya, N. Browning (Eds.), Mixed Ionic Electronic Conducting Perovskites for Advanced Energy Systems, Kluwer Academic Publishers, 2004, pp. 72–82.
[7] N. Orlovskaya, D. Steinmetz, S. Yarmolenko, D. Pai, J. Sankar, J. Goodenough, Phys. Rev. B 72 (2005), 014122-1-7.
[8] N. Orlovskaya, N. Gonzalez, J. Mater. Process. Manuf. Sci. 9 (53) (2000) 53–63.
[9] M.M. Natile, E. Ugel, C. Maccato, A. Glisenti, Appl. Catal. B. Environ. 72 (2007) 351–362.
[10] T. Fett, D. Munz, G. Thun, J. Am. Ceram. Soc. 81 (1998) 269–272.
[11] A. Nadai, Theory of Flow and Fracture of Solids, vol. 1, McGraw-Hill, New York, 1950 (Chapter 22).
[12] S.C. Hwang, C.S. Lynch, R.M. McMeeking, Acta Metal. Mater. 43 (1995) 2073–2084.
[13] J.L. Jones, M. Hoffman, J. Am. Ceram. Soc. 89 (2006) 3721–3727.
[14] K. Mehta, A.V. Virkar, J. Am. Ceram. Soc. 73 (1990) 567–574.
[15] D. Munz, T. Fett, Ceramics: Mechanical Properties, Failure Behaviour, Materials Selection, 1st ed., Springer, 2001, p. 8.
[16] T. Fett, W. Hartlieb, K. Keller, B. Knecht, D. Münz, W. Rieger, J. Nucl. Mater. 184 (1991) 39–46.
[17] J. Kübler, J. Woodtli, K. Berroth, in: J.R. Varner, V.D. Frechette, G.D. Quinn (Eds.), Fractography of Glasses and Ceramics III, The American Ceramic Society, 1996, p. 171.
[18] European Standard, EN 623-2, Advanced Technical Ceramics–Monolithic Ceramics—General and Textural properties, Part 2. Determination of Density and Porosity, September 1993.
[19] G.M. Gladysz, K.K. Chawla, Composites A 32 (2001) 173–178.
[20] preEN 843-2 redraft 3, Methods of test for advanced technical ceramics, Review of ENV 843-2, Determination of elastic moduli at room temperature, February 2004.
[21] J. Kübler, in: J.A. Salem, G.D. Quinn, M.G. Jenkins (Eds.), ASTM STP 1409, ASTM 2002, pp. 93–106.
[22] ASTM Designation: F 43-93, Standard Test Methods for Resistivity of Semiconductor Materials, October 1993.
[23] European Standard Final Draft, prEN 843-3, Advanced technical ceramics, Monolithic ceramics, mechanical properties at room temperature, Part 3: Determination of subcritical crack growth parameters from constant stressing rate flexural strength tests, November 2004.
[24] P.G. Radaelli, S.-W. Cheong, Phys. Rev. B 66 (2002), 66094408-1-9.
[25] C. Zobel, M. Kriener, D. Bruns, J. Baier, M. Grüninger, T. Lorenz, P. Reutler, A. Revcolevschi, Phys. Rev. B 66 (2002), 020402-1-4.
[26] S. Murata, S. Isida, M. Suzuki, Y. Kobayashi, K. Asai, K. Kohn, Physica B 263-264 (1999) 647–649.
[27] M.A. Korotin, S.Y. Ezhov, I.V. Solovyev, V.I. Anisimov, D.I. Khomskii, G.A. Sawatzky, Phys. Rev. B 54 (1996) 5309–5316.
[28] F.M. Figueiredo, F.M.B. Marques, J.R. Frade, Solid State Ionics 138 (2001) 173–182.
[29] B. Gilbu, H. Fjellvag, A. Kjekshus, Acta Chem. Scand. 48 (1994) 37.
[30] S. Uhlenbruck, F. Tietz, Mater. Sci. Eng. B 107 (2004) 277–282.
[31] D.I. Khomskii, G.A. Sawatzky, Solid State Commun. 102 (1997) 87–99.
[32] S. Stolen, F. Gronvold, H. Brinks, T. Atake, H. Mori, Phys. Rev. B 55 (1997) 14103–14106.
[33] J. Mastin, M.-A. Einarsrud, T. Grande, Chem. Mater. 18 (2006) 1680–1687.
[34] S. Miyoshi, J.-O. Hong, K. Yashiro, A. Kaimai, Y. Nigara, K. Kawamura, T. Kawada, J. Mizusaki, Solid State Ionics 161 (2003) 209–217.
[35] C.J. Howard, B.J. Kennedy, B.C. Chakoumakos, J. Phys.: Condens. Matter. 12 (2000) 349–365.

[36] G. Thornton, B.C. Tofield, A.W. Hewat, J. Solid State Chem. 61 (1986) 301–307.
[37] Y. Kobayashi, T. Mitsunaga, G. Fujinawa, T. Arii, M. Suetake, K. Asai, J. Harada, J. Phys. Soc. Jpn. 69 (2000) 3468–3469.
[38] S. Faaland, T. Grande, M.-A. Einarsrud, P.E. Vullum, R. Holmestad, J. Am. Ceram. Soc. 88 (2005) 726–730.
[39] M. Radovic, E. Lara-Curzio, L. Riester, Mater. Sci. Eng. A 368 (2004) 56–70.
[40] J.-S. Zhou, J.-Q. Yan, J.B. Goodenough, Phys. Rev. B 71 (2005), 220103(R)-1-4.
[41] R.J. Harrison, S.A.T. Redfern, Phys. Earth Planet. Int. 134 (2002) 253–272.
[42] C.M. Landis, J. Mech. Phys. Solids 51 (2003) 1347–1369.
[43] B.J. Dalgleish, R.D. Rawlings, J. Biomed. Mater. Res. 15 (1981) 527–542.
[44] S. Pathak, D. Steinmetz, J. Kuebler, A. Payzant, N. Orlovskaya, Ceram. Int., submitted for publication.